Brain-wide measurement of protein turnover with high spatial and temporal resolution

Boaz Mohar[1], Jonathan B. Grimm[1], Ronak Patel[1], Timothy A. Brown[1], Paul Tillberg[1], Luke D. Lavis[1], Nelson Spruston[1], Karel Svoboda[1,2]

1: HHMI Janelia Research Campus, Ashburn, VA; 2: Allen Institute for Neural Dynamics, Seattle, WA

Abstract

Cells regulate function by synthesizing and degrading proteins. This turnover ranges from minutes to weeks, as it varies across proteins, cellular compartments, cell types, and tissues. Current methods for tracking protein turnover lack the spatial and temporal resolution needed to investigate these processes, especially in the intact brain, which presents unique challenges. We describe a pulse-chase method (DELTA) for measuring protein turnover with high spatial and temporal resolution throughout the body, including the brain. DELTA relies on rapid covalent capture by HaloTag of fluorophores that were optimized for bioavailability *in vivo*. The nuclear protein MeCP2 showed brain region- and cell type-specific turnover. The synaptic protein PSD95 was destabilized in specific brain regions by behavioral enrichment. A novel variant of expansion microscopy further facilitated turnover measurements at individual synapses. DELTA enables studies of adaptive and maladaptive plasticity in brain-wide neural circuits.

Introduction

Cells regulate function by tuning transcription and translation to produce new proteins. Protein synthesis is balanced by protein degradation, which results in dynamic protein turnover[1]. In the brain, protein lifetimes range from tens of minutes of immediate early gene proteins[2] to months in the case of synaptic structural proteins[3]. Turnover rates vary by protein location or function, cell type, and brain region[4–6]. This dynamic process changes with environmental and behavioral conditions[6,7] and is modulated in neurodegenerative diseases[8]. Protein turnover is also required for animals to learn cognitive and motor tasks[9–11]. For example, learning is supported by long-term

changes in synaptic strength that require both protein synthesis[12,13] and degradation[14–16]. Protein turnover is regulated at multiple spatial scales in the brain. During learning and behavior, activity-dependent gene regulation is distributed throughout brain-wide neural circuits[17–19], but changes in synaptic strength are limited to active synapses[20–24], suggesting subcellular regulation of protein turnover. This combination of brain-wide and subcellular regulation calls for multiscale measurements of protein turnover *in vivo*.

Metabolic incorporation of modified amino acids followed by mass spectrometry allows the measurement of many proteins in parallel[25], but spatial resolution is limited to the level of brain regions (*e.g.*, cortex vs. cerebellum) or homogenate fractions (*e.g.*, cytoplasm vs. synaptosomes). In addition, results vary between individual studies[26]. Alternatively, fluorescent imaging methods allow labeling with different fluorophores at specific time points by fusing a tag with a protein of interest. This approach offers better spatial resolution, but remains difficult to deploy in the brain because of the need for epitope tags and labeled antibodies[27,28] or the self-labeling SNAP-tag system and existing associated substrates, which do not cross the blood brain barrier[29–31].

Here, we overcome these issues by using the HaloTag system (HT)[32] and cognate fluorescent ligands optimized for bioavailability, allowing the measurement of protein lifetimes in the brain and other tissues *in vivo*. We first developed procedures for efficient labeling of HT with a panel of Janelia Fluor (JF) dyes attached to the HaloTag ligand (HTL)[33–35] in the mouse brain. Using spectrally separable dyes, we then developed a pulse-chase protocol to estimate protein lifetimes *in vivo*, which we named DELTA (**D**ye **E**stimation of the **L**ifetime of pro**T**eins in the br**A**in). We used simulations and calibration measurements to assess the sensitivity and precision of DELTA. We then fused HaloTag protein to the nuclear transcriptional repressor protein MeCP2 and the synaptic scaffold protein PSD95 and measured the brain-wide protein turnover of these proteins at subcellular resolution. DELTA allows measurement of protein turnover with unprecedented spatial and temporal resolution.

Results

Measuring protein turnover *in vivo* with high spatial and temporal resolution

We first modeled how a pulse-chase paradigm could measure protein lifetime *in vivo* (**Fig. 1a**). We defined two populations of HaloTag fusion proteins (protein-HT): *P* denotes the labeled population with the initial dye infusion (pulse), and *C* denotes the newly synthesized protein labeled with a later, spectrally separable dye (chase). We assume that: (1) dye administrations are sufficient to saturate protein-HT, (2) dye clearance is much faster than protein turnover, and (3) protein degradation is exponential. The mean lifetime of the protein is then $\tau = \Delta T/\log(1/FP)$, where ΔT is the interval between the pulse and chase dye administration and FP is fraction of pulse-labeled part ($FP = P/[P + C]$). However, our assumptions may not be met in the context of real-life experiments and the consequences on measurements of turnover need to be evaluated. For example, incomplete labeling of the protein during the pulse dye injection could introduce a systematic under-estimation of lifetime. Alternatively, slow dye clearance would label newly synthesized protein and thus produce an over-estimate of lifetime.

To quantify these errors, our model (**Extended Data Fig. 1)** included both the dye kinetics (measured using *in vivo* imaging; **Supplementary Table 1**, **Extended Data Fig. 2)** and the dye-to-protein ratio as a measure of undersaturation or dye excess (dye/protein ratio of <1 or >1, respectively; **Fig. 1b**). We compared the estimated lifetime and the true lifetime using the following relation: $E=(\tau_{estimated} - \tau_{true})/\tau_{true} \times 100$. We found that undersaturation produces large errors, independent of protein lifetime. In contrast, dye excess produces small errors, except for proteins with very short lifetimes (on the order of, or shorter than the extrusion time of ~82 min; **Extended Data Fig. 2**). These results show that estimation errors are expected to be small if labeling is saturated and protein lifetime is longer than one quarter of the mean dye clearance time. Moreover, these biases would not change the relative measurements of protein lifetime across cell types, brain regions, or individual animals (see **Supplementary Note 1)**.

To find dyes that bind protein-HT efficiently in mouse brains *in vivo* (**Methods**; **Extended Data Fig. 3; Supplementary Fig. 1**) we screened different JF-HTL compounds[33–35]. We expressed green fluorescent protein tagged with HT (GFP-HT) in mouse brains *in vivo.* JF-HTL dyes (**Supplementary Table 2**) were injected retro-orbitally, and after 12–18 hours we perfused the brain with a spectrally orthogonal dye. With this approach, the unbound pulse dye has been cleared, protein degradation and synthesis are expected to be minimal, and the second dye will bind to the unlabeled protein (*i.e.*, undersaturated). Therefore, we used FP as a measure of the dye's ability to

saturate the protein-HT target. Two dyes, JF_{669}-HTL and JF_{552}-HTL, were particularly bioavailable *in vivo* and displayed uniform labeling in the brain (**Supplementary Note 2; Supplementary Fig. 2**).

Measuring cell type and brain region – specific turnover of the nuclear protein MeCP2

We next measured the lifetime of methyl-CpG binding protein 2 (MeCP2), an abundant nuclear protein implicated in chromatin remodeling in neurons and Rett syndrome[36–38]. We measured MeCP2 turnover by analyzing MeCP2-HT knock-in mice[39]. Previous MeCP2 lifetime using metabolic pulse-chase labeling provide a point of comparison for our method[6]. MeCP2 is a challenging case because it is expressed at high concentrations in all tissues. To assess saturation, JF_{669}-HTL was injected retro-orbitally (*P*), followed by perfusion of another dye ligand (C; JF_{585}-HTL) after one hour (**Extended Data Fig. 4a**). We imaged JF_{669}-HTL and JF_{585}-HTL fluorescence with subcellular resolution and at a brain-wide level. The lack of *C* staining indicated saturation with *P* dye in most harvested tissues, including most regions of the brain (**Extended Data Fig. 4b–h**). However, some brain regions with very dense cell body layers, were not saturated (*e.g.*, hippocampal CA1 region; **Extended Data Fig. 4i**). This is likely due to dye depletion and clearance of the dye before it could saturate these dense, MeCP2-HT-expressing structures. We therefore excluded these brain regions from analysis and focused on areas where MeCP2-HT was saturated by the pulse dye.

We sequentially injected highly bioavailable dyes (JF_{669}-HTL, JF_{552}-HTL), followed by perfusion of a third dye (JF_{608}-HTL) during harvesting of tissues (**Fig. 1c**). This allowed us to compile multiple estimates of protein lifetime from the same animal (Methods). After perfusion, the brain was sectioned and stained with DAPI to identify all nuclei, and immunofluorescence (IF) was used to classify cell types (**Fig. 1c-d**). We imaged JF_{669}-HTL, JF_{608}-HTL, and JF_{552}-HTL fluorescence with subcellular resolution and calculated *FP* for all neuronal nuclei across the brain of five MeCP-HT mice. We segmented MeCP2 nuclei using Ilastik[40] and converted the measurements to average protein lifetime under the assumption of a single exponential decay (**Methods**; **Fig. 1d**).

The lifetime of MeCP2 differed between brain regions. To assess the consistency of our method, we looked at pairwise correlations across animals for all commonly imaged brain regions

(**Fig. 1e**, left and middle panel). The average mean correlation across pairs was high compared to shuffled controls for three levels of region annotation representing different spatial scales (5, 10, and 50 regions) based on the Allen Brain Reference common coordinate framework (CCFv3; **Extended Data Fig. 5a-c**)[41]. The largest outlier was high MeCP2 stability in the cerebellum (**Fig. 1e**, right panel), in agreement with a previous study[6]. Imaging consecutive coronal slices of the same cortical region, we also saw similar lifetimes of MeCP2-HT in neurons to those in oligodendrocytes and microglia when looking at consecutive coronal slices on the same brain region (**Extended Data Fig. 5d-f)** contrary to other reports[7]. These results demonstrate that the pulse-chase paradigm enables measurements of protein lifetime at subcellular resolution and brain-wide scales. The lifetime of MeCP2-HT was consistent across animals under the same conditions, varied between brain regions, and was similar between different cell types in the same cortical region.

Turnover of PSD95 is accelerated by behavioral enrichment

We next investigated the brain-wide dynamics of PSD95, a synaptic scaffold abundant in post-synaptic densities of excitatory synapses[42], using knock-in mice expressing PSD95 fused with HT (PSD95-HT)[43]. Because our goal is analysis down to the level of individual synapses, we developed an improved dye-ligand: JFX_{673}-HTL (**Fig. 3a** and **Extended Data Fig. 6**). This dye is structurally similar to JF_{669}-HTL but contains deuterated pyrrolidine substituents instead of azetidines, an alteration that improves fluorophore brightness and photostability[35]. We discovered this modification maintained high bioavailability of its parent dye ligand, which is thought to be governed by chemical properties[34]. JFX_{673}-HTL saturated the HaloTag protein in the PSD95-HT knock-in mouse line (**Extended Data Fig. 6)**.

Next, we measured the effects of behavioral manipulations on the half-life of PSD95-HT (**Fig. 3b**), using dye-injection formulations optimized for saturating the abundant PSD95-HT (**Supplementary Note 3** and **Methods**). Mice were separated into two groups: animals in the control group (n=2) were housed in isolation and animals in a second group (n=4) were housed in pairs in an enriched environment (EE)[44,45]. At the time of separation into groups all mice received the pulse dye (JFX_{673}-HTL) and after two weeks mice were perfused with a spectrally orthogonal chase dye (JF_{552}-HTL). Brains were sectioned, imaged, registered to the Allen Brain Reference

(CCFv3), and PSD95 lifetime was calculated (**Fig. 3c**, **Methods**). The PSD95-HT lifetime differed between brain regions in both control and EE mice, as seen for example between cortical layers and hippocampal subfields (**Fig. 3d**; 1-way ANOVA, 6, F=105.91 p=6.7e-68). Looking more broadly, we observed significant variability across different brain regions regardless of behavioral enrichment (**Fig. 3e**; 1-way ANOVA, df=11, F=33.11, p=1.3e-51). Averaging across all brain regions, the brain-wide average half-life of PSD95 was more than a day shorter (~10%) in mice housed for two weeks in EE (**Fig. 3f**; average of all regions based on conditions: EE, magenta: 12.5±0.23 days n=4; control, green: 13.9±0.33 days n=2; ANOVA df=1, F=12.28 p=0.0248; individual animals in light colors).

To determine whether EE produced nonuniform effects across brain regions, we compared differences between EE and control animals. We observed that the isocortex had the largest difference (**Fig. 3g**, 1-way ANOVA, df=7, F=53.11 p=1.8e-55). We then looked at different cortical layers and hippocampal subfields. We found that although layer 1 had significantly higher PSD95-HT stability, deeper layers destabilized significantly more with EE (**Fig. 3h**; 1-way ANOVA, df=6, F=3.4 p=0.003).

Next, we investigated the turnover of PSD95-HT at individual synapses. This requires an approximately four-fold better resolution than permitted by the classical diffraction limit. Expansion microscopy (ExM)[46] permits this four-fold enhancement, but uniform expansion requires dissolving the native tissue structure through proteolysis or strong denaturation, which we found to cause loss of signal (~50% for antibodies or fluorescent proteins). Therefore, we developed an ExM protocol that would enable two-fold expansion without proteolysis or strong protein denaturation. We imaged the expanded sample with Airyscan confocal microscopy[47], which provides another two-fold improvement in resolution, yielding an overall four-fold resolution enhancement (**Methods**). Our use of bright and photostable small-molecule dyes, combined with the lack of any protein disruption during expansion enabled measurements of turnover at individual synapses. We applied this method to different brain regions of one coronal section and were able to measure turnover in single synapses of layer 1 and CA1 which had a longer lifetime than CA3 synapses (**Fig. 3i; Supplementary Movie 3,4**).

Discussion

DELTA enables measurement of the protein lifetime with unprecedented temporal and spatial precision, throughout the body, including in the brain, which presents special challenges. Using *in vivo* calibration measurements and *in situ* modeling, we defined the appropriate conditions for this pulse-chase paradigm in mice. We also introduced a new dye, JFX_{673}-HTL, with ideal properties for pulse-chase measurements *in vivo*. Consistent with previous measurements using metabolic labeling, we found that MeCP2-HT protein turnover is slower in the cerebellum compared to other brain areas. We then measured the lifetime of the major excitatory synaptic scaffold protein PSD95 at a range of spatial scales from brain regions to single synapses. We found that PSD95-HT is destabilized by enriched experience, with cortical layers 2–5 as a major locus of plasticity.

DELTA is complementary to mass spectroscopy (MS) based methods for measuring protein lifetime, with each method having distinct advantages and disadvantages. MS can measure 1000s of proteins in parallel but provides only low spatial resolution. DELTA provides much higher spatial resolution but can only be used to analyze one protein at a time, limiting throughput and making simultaneous multi-protein measurements challenging. MS requires expensive equipment, whereas DELTA requires genetically engineered animals and tests of protein saturation (**Fig. 1b**) for each new knock-in mouse.

DELTA presents several advantages over previous methods and opportunities for extensions. First is the range of spatial resolution—from millimeters to ~100 nanometers—that can be achieved with a *post hoc* imaging-based approach. Second is the ability to combine turnover measurements with other imaging-based molecular methods such as fluorescence *in situ* hybridization (FISH)[48] or immunofluorescence (IF). We have demonstrated IF for the identification of cell types. It could also be used to identify other proteins to identify synaptic pathways or other subcellular compartments. Additionally, DELTA could be combined with other approaches to examine the relationships between neural activity and protein turnover by *in vivo* expression of indicators or actuators of neural activity.

DELTA could also be used to examine learning-related changes in synaptic proteins across the brain, including turnover measurements at the level of brain regions, cell types, specific input pathways, and individual synapses. This could also be done in both healthy mice and animal

models of neurological disorders such as depression. Another application could involve measurements of activity *in vivo* with *ex vivo* protein lifetime measurements in the same cells to understand the effect of the history of activity on the changes in protein lifetime. Thus, this new method could help the field identify brain-wide changes involved in adaptive and maladaptive processes in an unbiased and high-thruput fashion.

Methods

Materials

Purified HaloTag protein (#G4491) was purchased from Promega (Madison, Wisconsin). Pluronic F127 (#P3000MP), DMSO anhydrous (#D12345), TEMED (N,N,N′,N′-tetramethylethylenediamine; #15524010), APS (Ammonium Persulfate; #AAJ7632209), and AcX (Acryloyl-X SE; #A20770) were purchased from Thermo Fisher Scientific (Rockville, MD). Acrylamide (#1610140) and bis-acrylamide (#1610142) were purchased from Bio-rad (Hercules, CA). To get sodium acrylate we neutralized acrylic acid purchased from TCI (Portland, OR; #A0141) with sodium hydroxide as previously described[49]. 4HT (4-Hydroxy-TEMPO; #176141-5G) was purchased from Sigma (Saint Louis, MO).

Animals

All procedures were performed in accordance with protocols approved by the Janelia Institutional Animal Care and Use Committee. Wild type mice (C57Bl/6J RRID:IMSR_JAX:000664; both male and female) were housed in a 12:12 reverse light:dark cycle. MeCP2-HT[50] and PSD95-HT[43] knock-in mice of either sex were used. However, comparisons were never made between males and females for MeCP2-HT mice.

Virus, dye injections and tissue processing

To evaluate the ability of JF dyes' to saturate HT proteins in the brain we needed sparse expression of an HT-labeled protein. We chose to express HaloTag-EGFP (HT-GFP) as many JF dyes are red or far red. Sparse brain expression and dye delivery were achieved using retro-orbital (RO) injections (Yardeni et al., 2011). Dye preparation[51], dye injections[52], and the histological preparations[53] are also described on protocols.io . HT-GFP virus was prepared using a PHP.eB AAV capsid (Chan et al. 2017) and a synapsin promoter. 100 µl of virus (titer of 4e11 GC/mL)

was injected RO. An mKate-HaloTag was used to avoid cross- talk between the GFP and the JF_{525}-HTL dye. RO dye injections (Pulse) were performed 3-5 weeks after virus injection. Most injections were prepared by dissolving 100 nmol of dye in 20 µl DMSO followed by 20 µl of 20% PF127 in DMSO and 60 µl of PBS except when otherwise noted (Suppıemental table 2). Twenty-four hours after dye injection, animals were perfused with 50 ml of 4% PFA in 0.1 M PB and 50 nmol of an orthogonal dye. The brains were post-fixed in 4% PFA in 0.1 M PB overnight at 4ºC and washed three times in PBS for 15 minutes. 100 µm coronal sections were cut and floated in 24 well plates followed by 4h DAPI staining (0.6 µM in PBS) and washed 3 times for 15 minutes in PBS. For animals with visible fluorescence from the in-vivo injection, every 4th slice was mounted for imaging; for animals where no fluorescence was observed, every 24th slice was mounted and imaged. See Supplementary table 2 for details of dyes and mounting of each of the animals in the study.

Expansion Microscopy

After sectioning, coronal sections were anchored with AcX (33 mg/ml) in PBS for one hour. Then they were moved to gelation solution containing: 2.7 M acrylamide, 0.2 M sodium acrylate, 200 µg/mL bis, PBS (1×), 2 mg/mL APS, 2 mg/mL TEMED, and 20 µg/mL 4HT. They were incubated on ice, shaking, for 30 minutes before being moved to gelation chambers and 37° C for one hour. After gelation, excess gel was dissected, and the tissue was recovered in pure water. After three one-hour washes in pure water, the slices were expanded ~2x without disruption or cracks. These sections were moved to a 6-well glass-bottom plate (Cellvis #P06-1.5H-N, Mountain View, CA). In order to flatten and immobilize the sections, 4 dabs of silicon grease were applied around the section and a 22x22 mm square #2 coverslip (Corning #2855-22, Corning, NY) was pressed from above. If needed, poly-L-lysine 0.2mg/ml (Sigma #P1524-25MG) with Photo-Flo 200 (1:500 from stock; #74257 Electron Microscopy Sciences, Hatfield, PA) could be applied to the bottom of the well before the sections are placed to better immobilize the gels.

Whole brain coronal section imaging

To image 6-20 coronal sections of tens of animals (i.e., hundreds of sections), we needed a high-throughput imaging platform. We used a confocal slide scanner consisting of a TissueFAXS 200 slide feeder (Tissuegnostics, Germany) and a SpectraX light engine (Lumencor) with the

following peak powers and excitation filters: V – 395nm-400mW (395nm/25nm), C – 475nm-480mW (475nm/34nm), G/Y – lightpipe (585nm/35nm), R – 619nm-629mW (635nm/22nm). These were delivered by a lightguide to a Crest X-Light V2 confocal spinning disc microscope (Crestoptics; 60um pinhole spinning disk) with the following dichroics: T425lpxr, T495lpxt, T600lpxr, T660lpxr and emission filters: ET460nm/50nm, ET525nm/50nm, ET625nm/30nm, ET700nm/75nm. The emission light was collected with Zeiss objectives: EC Plan-Neofluar 2.5x/0.085 M27 for tissue detection, EC Plan-Neofluar 10x/0.3 M27 for MeCP2 and PSD95 animals (**Fig. 2c-h; Extended Data Fig. 4; Supplementary Fig. 5**) and a Plan-Apochromat 20x/0.8 M27 for virally injected animals (**Extended Data Fig. 3; Supplementary Fig. 1,2**). Detection was done using a Zyla 5.5 sCMOS camera (Andor). Acquisition of the coronal sections was performed after semi-automated tissue detection and by using multiple autofocusing points per section (5x5 and 3x3 grids for 20x and 10x objective acquisitions accordingly). For virally transfected animals, three z-planes were imaged, and z projected with a 7 µm spacing. For MeCP2 and PSD95 animals a single plane was imaged.

High resolution imaging

To segment individual nuclei of MeCP2 expression (**Fig. 1d-f**; **Extended Data Fig. 5**) or single synapses expressing PSD95 (**Fig. 2i**), higher resolution imaging was needed. For MeCP2 imaging we used a Zeiss LSM 880 (Blackwood, NJ) with an EC Plan-Neoflour 40x/1.3NA oil objective and a voxel size of 0.25x0.25x0.5 µm. We acquired 21 z planes and 5 channels in 3 tracks. Detection [excitation] wavelengths were as follows (all in nm): Track 1 - DAPI: 410-489 [405]- DAPI, JF_{612}: 624-668 [594]; Track 2 IF: 493-551nm [488], JF_{669}: 680-758 [633]; Track 3 JF_{552}: 553-588 [561]. For PSD95 imaging we used a Zeiss LSM 980 with Airyscan and a C-Apochromat 40x/1.2 water dipping objective. The resulting pixel size after Airyscan processing was 57x57x230 nm. We acquired 23 z sections with two channels, 561 nm illumination for JF_{552} and 633 nm illumination for JFX_{673}. A full z-stack was acquired for the far-red channel followed by the red channel.

Image analysis

JF Dye screening

We wanted to determine the amount of saturation for each dye injected *in vivo* (**Extended Data Fig. 3; Supplemental Fig. 1-3**). However, saturation needs to consider the amount of total protein (total = C+P), so fraction pulse (FP) was used as a measure of saturation: FP = P/(C+P). Doing a pixel-wise analysis would not be sufficient as there are background signals that would change based on the imaged channel and brain region. Here, unlike knock-in animals, there is variability in the expression pattern across animals that could also affect the background (neruopil) in which the cells reside. We thus chose to do a mask-based analysis for cells along with a local background component that would avoid these confounds. To set masks, we imported 2x down-sampled images with 3 channels (GFP-HT/P/C) into Ilastik's pixel classification workflow (Berg et al., 2019). The workflow was manually trained to segment cell bodies, dendrites, different types of neuropil signal and different imaging and tissue artifacts. The pixel probabilities maps for cells, combined with the raw data, were then imported to a second, object-classification workflow in Ilastik. This workflow was used to classify each mask as a GFP-HT-expressing cell or not. A Matlab script was used to calculate each mask's value in the three channels and calculate a local background as well. The local background estimation excluded pixels that belonged to other non-neuropil trained categories (other cells, dendrites, etc.) from the first Ilastik workflow (**Extended Data Fig. 3c; Supplemental Fig. 1**). Each mask was calculated a background subtracted value and converted to μM dye concentration using an independent calibration obtained under the same imaging conditions (**Supplemental Fig. 3**). The FP was calculated after conversion to μM dye, where FP values closer to 1 indicate saturation.

MeCP2

To segment MeCP2-HT nuclei and categorize them to cell types using IF, a modified Ilastik classification pipeline was used (**Fig. 1c,d; Extended Data Fig. 5**). First, the five imaged channels (DAPI, Pulse, Chase1, Chase2, IF) were each normalized from 0 to 1 using the top and bottom 0.3% of the histogram. Second, a mean of all three imaged JF dyes was used to make a 3-channel image (DAPI, mean of all JF dyes, IF). This was used in the pixel classification workflow in Ilastik. We used training data from all three types of IF used (NeuN, Iba1 and SOX10). The resulting nuclei probability maps in combination with the 3-channel images were used by three independent object classification workflows in Ilastik, one for each IF type. The output of these three workflows were masks that of IF-positive nuclei for each cell type. These were used as described above to

extract FP after conversion to μM dye using calibration measurement's done under the same imaging conditions. Next, a mean lifetime (τ) was calculated with the assumption of a single exponential decay given our pulse-chase interval (ΔT): $\tau = \Delta T / \log\left(\frac{1}{FP}\right)$.

Brain-wide PSD95 analysis

To assign PSD95 lifetimes across the brain we performed a pixel-based analysis (**Fig. 1b-h**), as there is no way to segment individual objects (synapses) from our low-resolution imaging. As with MeCP2, we converted our images to 3-channel images (DAPI/P/C) after a 2× downsampling and normalization to saturate the 0.3% top and bottom of each channel's histogram. These were the imported to an ilastik pixel-classification workflow that was trained to detect places where synapses are a meaningful signal (i.e., excluding non-tissue, artifacts, ventricles). The result was used as a mask on the original data. As in MeCP2 analysis, each pixel was converted to a lifetime estimate with the assumption of a single exponential decay after conversion to μM dye concentration using calibration curves imaged under the same conditions.

Expansion microscopy PSD95

After acquisition using the Airyscan detector array we used Zen Blue software (Zeiss) to process the images using a 3d reconstruction of each channel with automated strength. The Airyscan-processed images were registered across channels as they were acquired sequentially. Shifts between channels were under 3 pixels. The resulting 2-channel image was normalized and used as input to an Ilastik pixel classification pipeline trained to separate synapses from the background. The resulting probability images with the normalized data were used in a second Ilastik object segmentation pipeline. Here synapses were classified as simple (single line) or complex (rings, multiple curves). Both classes were used (**Fig. 2i**). As we had segmented objects, we could subtract a local background, use a calibration to convert the values to μM dye and get an estimated lifetime assuming a single exponential decay.

Alignment to CCF

To align both MeCP2 and PSD95 lifetime measurements to the Allen CCF a two-step procedure was used. First a downsampled (max 1.5Mb with png) 24-bit RGB image of each section was generated. It was loaded with QuickNII[54] and aligned to version 3 of the Allen CCF at 25 μm

resolution. This was able to account for the cutting angle, a global scaling factor in DV and ML axis and the AP location of each section. Output from QuickNII was used for a manual non-rigid alignment with VisuAlign[55]. The main markers for alignment were the edges of the section, the ventricles and fiber tracks. The output from VisuAlign was another RGB image in which each color is assigned to an Allen Institute CCF id. These images were loaded and interpolated to the original size of each section enabling the assignment of each MeCP2 nuclei and PSD95 pixel to a CCF id. As the PSD95 analysis was pixel based, we excluded any pixel belonging to the root or any part of the CCF tree under fiber tracks or ventricular system.

Dye clearance

Cranial windows were made over either ALM or V1 (centered on - 2.5 mm lateral, + 0.5 mm anterior from lambda) and a headbar was attached posterior to the window as described previously[56]. Animals were anesthetized in 1% isoflurane and kept at 37C with a heating pad. The optical setup was the same as described previously[57], with a custom wide-field fluorescence microscope (Thorlabs) and a sCMOS camera (Hamamatsu Orca Flash 4.0 v3). Details of illumination, objectives and filters are presented in Supplementary Table 1. A baseline image was acquired before dye injection. Both the baseline and following timepoints were acquired as movies of 40-50 frames at 5 Hz. This was done to reduce the chances of saturating pixels on the camera at the peak on the injection while still being above electrical noise at baseline conditions. The animal was then removed from head fixation and injected with dye. After dye injection it was quickly returned to head fixation, the field of view was compared to a baseline image under room lights and was then imaged for up to four hours in intervals of 2 minutes to 20 minutes to cover the fast decay part of the dye clearance. The animal was then recovered and reimaged for up to 24 h in intervals of 4-12 h.

The images were analyzed using a custom Matlab script (Github). Briefly, each movie was averaged, and a manual ROI was defined (**Extended Data Fig. 2b**). The pixel-averaged mean was fitted to a double exponential: $F = \boldsymbol{a} * \boldsymbol{e}^{-1/\tau_1} + \boldsymbol{b} * \boldsymbol{e}^{-1/\tau_2} + \boldsymbol{c}$. Population averages were computed by binning all 11 experiments together. In cases where the rising phase of the injection was captured, an offset was used to start the fitting from the highest timepoint.

Carotid artery dye infusion

To measure the infusion kinetics of JF dyes, we needed a way to control the rate of infusion while imaging dye accumulation in the brain through a cranial window (**Supplemental Fig. 4**). We used two C57Bl/6j animals with a Common Carotid Artery vascular catheterization. These were ordered from Charles Rivers as a surgical service. They were flushed with saline and 50% sucrose lock solution every 7 days. A cranial window was done 7 days after catheterization as described above. 7 days after the cranial window surgery a pump with JF dye was connected to the carotid artery line. The initial pump rate was 20 ul/min followed by 40 ul/min and 80 ul/min. Imaging conditions were the same as for dye clearance experiments (0.2 s exposure) but imaged continuously for each injection speed. Data were time averaged to 1 s (5 timepoints) and a manual ROI was drawn. Time-averaged fluorescence values were trimmed to times the pump was running and fit with a linear fit (including intercept). The values reported are the slopes of the fit.

Modeling dye clearance effects on saturation

We wanted to test the hypothesis that given a fixed amount of dye to inject, faster injections would lead to more dye captured in the brain. We considered a simple model where a single position in space (x position 1) is a blood vessel from which dye can enter the system and diffuse in 1D simulated by a time march (using Fourier's equation). To avoid edge conditions (Dirichlet boundary conditions were simulated) care was taken to simulate all relevant dye diffusion away from the edge. Both dye injection and clearance were simulated at the same arbitrary rate (dt). All simulations had the same total amount of dye injected and a constant amount of dye was cleared from the vessel at a rate of 1AU/dt. Different simulations had different injection rates (2-10 AU/dt) and the width of dye distribution was measured as being the width in dx at 90% of the known saturation value. Code is available online (GitHub).

Modeling protein turnover measurements with DELTA

Pulse-chase experiments were modeled using the SimBiology package in Matlab (Mathworks; GitHub link). Briefly, lifetimes of the target HT-protein synthesis were simulated. Each new protein could either degrade (at the same rate of synthesis modeled) or attach to a HaloTag ligand dye molecule (Pulse or Chase, dye collectively). The dye binding kinetics were set to be nearly instantaneous as they are several orders of magnitude higher than synthesis/degradation. Binding

kinetics were identical to both the Pulse and Chase. Degradation rates of the HT-protein with dye complexes were the same as for the protein alone.

The dye injection kinetics were neglected (i.e., instantaneous injection). Dye clearance kinetics were modeled as two compartments (named Brain & Lipids) with degradation from the Brain compartment. This was done to account for the multi-exponential decay measured *in vivo*. The Brain compartment was set to have a volume of 1 ml; the equilibrium constant between the compartments, the volume of the Lipids compartment and the degradation time constant were fitted using the JF-dyes clearance data (**Extended Data Fig. 1,2**). This fitting was done in the absence of a HT-protein. After fitting each dye experiment, the confidence intervals around the mean value of the three fitted parameters were used as the limits of a uniform distribution to simulate the range of possible dye clearance kinetics.

Dye solubility

Formulations for solubility measurements of JF dyes were prepared in following manner. (i) 30% Captisol formulation was made with 300 mg Captisol® (β-Cyclodextrin Sulfobutyl Ethers, sodium salts) (NC-04A-180186, Cydex Pharmaceuticals) dissolved in 1 ml of sterile water (Molecular Biology Grade Water, Corning) to make a 30% solution. 100 µl of this solution was added to 100 nmol of dry JF dye. (ii) 30% Captisol + Pluronic formulation was made by mixing 30% Captisol solution with Pluronic™ F-127 (P3000MP, Invitrogen) in 80:20 ratio. 100 µl of prepared solution was added to 100 nmol of dry JF dye. (iii) DMSO + Pluronic formulation was made with DMSO (D2650, Sigma Aldrich), Pluronic ™ F-127 and sterile saline (0.9 % sodium chloride) mixed in 20:20:60 ratio. 100 µl from the prepared solution was added to 100 nmol of dry JF dye. (iv) DMSO only formulation was made by adding 100 µl of DMSO was added to 100 nMoles of dry JF dye to bring it to final concentration of 1 mM.

The prepared JF dye formulations were vortexed briefly followed by a bath sonication (Branson 1200 model) for 5 minutes. The dye solutions were placed on the agitator for 72 h to ensure solubilization. Absorbance measurements on the dye solutions were made using a spectrometer (Cary 100 UV-Vis, Agilent Technologies), and the final concentration was determined from known extinction coefficients of JF dyes as defined by Grimm et al. [33–35].

Data and Code availability

Both metadata and raw data are available through the Open Science Foundation project associated with this paper. Protocols are available as a collection on protocols.io. Code used for analysis is available on GitHub.

References

1. Alberts, B. *et al. Essential cell biology*. (W. W. Norton & Company, 2019).
2. Soulé, J. *et al.* Balancing Arc synthesis, mRNA decay, and proteasomal degradation: maximal protein expression triggered by rapid eye movement sleep-like bursts of muscarinic cholinergic receptor stimulation. *J. Biol. Chem.* **287**, 22354–22366 (2012).
3. Heo, S. *et al.* Identification of long-lived synaptic proteins by proteomic analysis of synaptosome protein turnover. *Proc. Natl. Acad. Sci.* **115**, E3827–E3836 (2018).
4. Alvarez-Castelao, B., Schanzenbächer, C. T., Langer, J. D. & Schuman, E. M. Cell-type-specific metabolic labeling, detection and identification of nascent proteomes in vivo. *Nat. Protoc.* **14**, 556–575 (2019).
5. Cohen, L. D. & Ziv, N. E. Neuronal and synaptic protein lifetimes. *Curr. Opin. Neurobiol.* **57**, 9–16 (2019).
6. Fornasiero, E. F. *et al.* Precisely measured protein lifetimes in the mouse brain reveal differences across tissues and subcellular fractions. *Nat. Commun.* **9**, 1–17 (2018).
7. Dörrbaum, A. R., Kochen, L., Langer, J. D. & Schuman, E. M. Local and global influences on protein turnover in neurons and glia. *eLife* **7**, e34202 (2018).
8. Paterson, R. W. *et al.* SILK studies — capturing the turnover of proteins linked to neurodegenerative diseases. *Nat. Rev. Neurol.* **15**, 419–427 (2019).
9. Flexner, J. B., Flexner, L. B. & Stellar, E. Memory in Mice as Affected by Intracerebral Puromycin. *Science* **141**, 57–59 (1963).

10. Luft, A. R., Buitrago, M. M., Ringer, T., Dichgans, J. & Schulz, J. B. Motor Skill Learning Depends on Protein Synthesis in Motor Cortex after Training. *J. Neurosci.* **24**, 6515–6520 (2004).
11. Park, H. & Kaang, B.-K. Balanced actions of protein synthesis and degradation in memory formation. *Learn. Mem.* **26**, 299–306 (2019).
12. Kelleher, R. J., Govindarajan, A., Jung, H.-Y., Kang, H. & Tonegawa, S. Translational Control by MAPK Signaling in Long-Term Synaptic Plasticity and Memory. *Cell* **116**, 467–479 (2004).
13. McGaugh, J. L. Memory--a Century of Consolidation. *Science* **287**, 248–251 (2000).
14. Fioravante, D. & Byrne, J. H. Protein degradation and memory formation. *Brain Res. Bull.* **85**, 14–20 (2011).
15. Fonseca, R., Vabulas, R. M., Hartl, F. U., Bonhoeffer, T. & Nägerl, U. V. A Balance of Protein Synthesis and Proteasome-Dependent Degradation Determines the Maintenance of LTP. *Neuron* **52**, 239–245 (2006).
16. Lee, S.-H. *et al.* Synaptic Protein Degradation Underlies Destabilization of Retrieved Fear Memory. *Science* **319**, 1253–1256 (2008).
17. DeNardo, L. A. *et al.* Temporal evolution of cortical ensembles promoting remote memory retrieval. *Nat. Neurosci.* **22**, 460–469 (2019).
18. Roy, D. S. *et al.* Brain-wide mapping reveals that engrams for a single memory are distributed across multiple brain regions. *Nat. Commun.* **13**, 1799 (2022).
19. Ye, L. *et al.* Wiring and Molecular Features of Prefrontal Ensembles Representing Distinct Experiences. *Cell* **165**, 1776–1788 (2016).
20. Bliss, T. V. & Lomo, T. Long-lasting potentiation of synaptic transmission in the dentate area of the anaesthetized rabbit following stimulation of the perforant path. *J. Physiol.* **232**, 331–356 (1973).
21. Frey, U. & Morris, R. G. M. Synaptic tagging and long-term potentiation. *Nature* **385**, 533–536 (1997).
22. Harvey, C. D. & Svoboda, K. Locally dynamic synaptic learning rules in pyramidal neuron dendrites. *Nature* **450**, 1195–1200 (2007).

23. Matsuzaki, M., Honkura, N., Ellis-Davies, G. C. R. & Kasai, H. Structural basis of long-term potentiation in single dendritic spines. *Nature* **429**, 761–766 (2004).

24. Nabavi, S. *et al.* Engineering a memory with LTD and LTP. *Nature* **511**, 348–352 (2014).

25. Chen, X., Wei, S., Ji, Y., Guo, X. & Yang, F. Quantitative proteomics using SILAC: Principles, applications, and developments. *PROTEOMICS* **15**, 3175–3192 (2015).

26. Alvarez-Castelao, B. & Schuman, E. M. The Regulation of Synaptic Protein Turnover. *J. Biol. Chem.* **290**, 28623–28630 (2015).

27. Butko, M. T. *et al.* Fluorescent and photo-oxidizing TimeSTAMP tags track protein fates in light and electron microscopy. *Nat. Neurosci.* **15**, 1742–1751 (2012).

28. Lin, M. Z., Glenn, J. S. & Tsien, R. Y. A drug-controllable tag for visualizing newly synthesized proteins in cells and whole animals. *Proc. Natl. Acad. Sci.* **105**, 7744–7749 (2008).

29. Bojkowska, K. *et al.* Measuring In Vivo Protein Half-Life. *Chem. Biol.* **18**, 805–815 (2011).

30. Hawkins, B. T. & Egleton, R. D. Fluorescence imaging of blood-brain barrier disruption. *J. Neurosci. Methods* **151**, 262–267 (2006).

31. Keppler, A. *et al.* A general method for the covalent labeling of fusion proteins with small molecules in vivo. *Nat. Biotechnol.* **21**, 86–89 (2003).

32. Los, G. V. *et al.* HaloTag: a novel protein labeling technology for cell imaging and protein analysis. *ACS Chem. Biol.* **3**, 373–382 (2008).

33. Grimm, J. B. *et al.* A general method to fine-tune fluorophores for live-cell and in vivo imaging. *Nat. Methods* **14**, 987–994 (2017).

34. Grimm, J. B. *et al.* A general method to optimize and functionalize red-shifted rhodamine dyes. *Nat. Methods* **17**, 815–821 (2020).

35. Grimm, J. B. *et al.* A General Method to Improve Fluorophores Using Deuterated Auxochromes. *JACS Au* **1**, 690–696 (2021).

36. Ehrhart, F. *et al.* Rett syndrome – biological pathways leading from MECP2 to disorder phenotypes. *Orphanet J. Rare Dis.* **11**, (2016).

37. Qiu, Z. *et al.* The Rett Syndrome Protein MeCP2 Regulates Synaptic Scaling. *J. Neurosci.* **32**, 989–994 (2012).

38. Zimmermann, C. A., Hoffmann, A., Raabe, F. & Spengler, D. Role of Mecp2 in Experience-Dependent Epigenetic Programming. *Genes* **6**, 60–86 (2015).

39. Piccolo, F. M. *et al.* Mecp2 Nuclear Dynamics in Live Neurons Results from Low and High Affinity Chromatin Interactions. *SSRN Electron. J.* (2019) doi:10.2139/ssrn.3376659.

40. Berg, S. *et al.* ilastik: interactive machine learning for (bio)image analysis. *Nat. Methods* **16**, 1226–1232 (2019).

41. Wang, Q. *et al.* The Allen Mouse Brain Common Coordinate Framework: A 3D Reference Atlas. *Cell* **181**, 936-953.e20 (2020).

42. Cho, K.-O., Hunt, C. A. & Kennedy, M. B. The rat brain postsynaptic density fraction contains a homolog of the drosophila discs-large tumor suppressor protein. *Neuron* **9**, 929–942 (1992).

43. Masch, J.-M. *et al.* Robust nanoscopy of a synaptic protein in living mice by organic-fluorophore labeling. *Proc. Natl. Acad. Sci.* **115**, E8047–E8056 (2018).

44. Nithianantharajah, J. & Hannan, A. J. Enriched environments, experience-dependent plasticity and disorders of the nervous system. *Nat. Rev. Neurosci.* **7**, 697–709 (2006).

45. Rosenzweig, M. R. & Bennett, E. L. Effects of differential environments on brain weights and enzyme activities in gerbils, rats, and mice. *Dev. Psychobiol.* **2**, 87–95 (1969).

46. Chen, F., Tillberg, P. W. & Boyden, E. S. Expansion microscopy. *Science* **347**, 543–548 (2015).

47. Huff, J. The Airyscan detector from ZEISS: confocal imaging with improved signal-to-noise ratio and super-resolution. *Nat. Methods* **12**, i–ii (2015).

48. Wang, Y. *et al.* EASI-FISH for thick tissue defines lateral hypothalamus spatio-molecular organization. *Cell* **184**, 6361-6377.e24 (2021).

49. Damstra, H. G. *et al.* Visualizing cellular and tissue ultrastructure using Ten-fold Robust Expansion Microscopy (TREx). *eLife* **11**, e73775 (2022).

50. Piccolo, F. M. *et al.* Mecp2 Nuclear Dynamics in Live Neurons Results from Low and High Affinity Chromatin Interactions. *SSRN Electron. J.* (2019) doi:10.2139/ssrn.3376659.

51. Mohar, B. Preparation of JF dye for retro-orbital injection in mice. *protocols.io* https://www.protocols.io/view/preparation-of-jf-dye-for-retro-orbital-injection-5u4g6yw (2019).

52. Mohar, B. *Retro-orbital injection of virus or dye in mice v1*. https://www.protocols.io/view/retro-orbital-injection-of-virus-or-dye-in-mice-5udg6s6 (2019) doi:10.17504/protocols.io.5udg6s6.

53. Mohar, B. & Copeland, M. *Protocol for mouse perfusion with dye, DAPI staining, and slide preparation v1*. https://www.protocols.io/view/protocol-for-mouse-perfusion-with-dye-dapi-stainin-59jg94n (2019) doi:10.17504/protocols.io.59jg94n.

54. QuickNII. (2022).

55. VisuAlign. (2021).

56. Goldey, G. J. *et al.* Removable cranial windows for long-term imaging in awake mice. *Nat. Protoc.* **9**, 2515–2538 (2014).

57. Abdelfattah, A. S. *et al.* Bright and photostable chemigenetic indicators for extended in vivo voltage imaging. *Science* **365**, 699–704 (2019).

58. Yardeni, T., Eckhaus, M., Morris, H. D., Huizing, M. & Hoogstraten-Miller, S. Retro-orbital injections in mice. *Lab Anim.* **40**, 155–160 (2011).

59. Holtmaat, A. *et al.* Long-term, high-resolution imaging in the mouse neocortex through a chronic cranial window. *Nat. Protoc.* **4**, 1128–1144 (2009).

60. Trachtenberg, J. T. *et al.* Long-term in vivo imaging of experience-dependent synaptic plasticity in adult cortex. *Nature* **420**, 788–794 (2002).

61. Walther, D. M. & Mann, M. Accurate Quantification of More Than 4000 Mouse Tissue Proteins Reveals Minimal Proteome Changes During Aging *. *Mol. Cell. Proteomics* **10**, S1–S7 (2011).

62. Zhao, Y., Denner, L., Haidacher, S. J., LeJeune, W. S. & Tilton, R. G. Comprehensive analysis of the mouse renal cortex using two-dimensional HPLC – tandem mass spectrometry. *Proteome Sci.* **6**, 15 (2008).

63. Chan, K. Y. *et al.* Engineered AAVs for efficient noninvasive gene delivery to the central and peripheral nervous systems. *Nat. Neurosci.* **20**, 1172–1179 (2017).

64. Verkhusha, V. V. *et al.* High Stability of Discosoma DsRed As Compared to Aequorea EGFP. *Biochemistry* **42**, 7879–7884 (2003).

65. Caujolle, F., Caujolle, D., Bouyssou, H. & Calvet, M. M. [TOXICITY AND PHARMACOLOGICAL APTITUDES OF DIMETHYLSULFOXIDE]. *Comptes Rendus Hebd. Seances Acad. Sci.* **258**, 2224–2226 (1964).

66. Krenzlin, H., Lorenz, V., Danckwardt, S., Kempski, O. & Alessandri, B. The Importance of Thrombin in Cerebral Injury and Disease. *Int. J. Mol. Sci.* **17**, 84 (2016).

Acknowledgments

Histology: Benjamin Foster, Monique Copeland, Amy Hu, Susan Michael; Imaging core: Michael DeSantis, Damien Alcor; Vivarium: Gillian Harris, Mariam Rose, Sarah Lindo; Viral core: PHP virus; T3 (bleaching): Ariana Tkachuk; Open chemistry: Anastasia Osowski, Katie Holland; GFP-HT virus: Eric Schreiter; MeCP2-HT animal: James Liu; PSD95-HT animal: Seth Grant; Clearance imaging: Amrita Singh

Figures

Figure 1 – Measurement of protein turnover *in vivo*, demonstrated with MeCP2

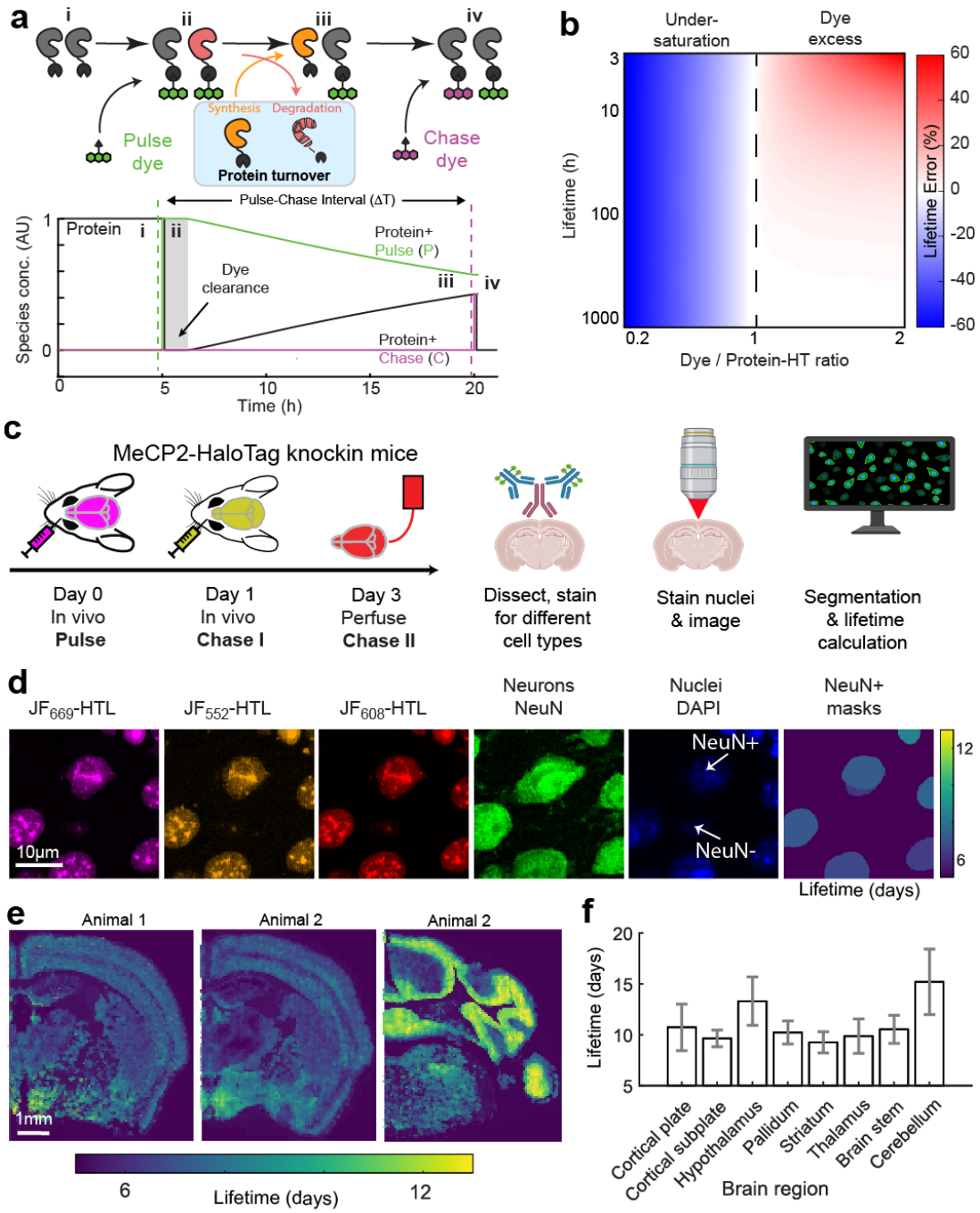

a, Schematics showing dye capture by a protein modified with a HaloTag (HT). (i) Before the injection of the first dye-ligand (pulse), there is no label on the protein (black line). (ii) After injection of the first dye (dashed green line at 5 h), all proteins are labeled with the pulse (solid green line). (iii) during the pulse-chase interval some proteins degrade, and others are synthesized (termed protein turnover) but are unlabeled. (iv) Injecting a spectrally separate dye (dashed magenta line at 20 h) captures the newly synthesized fraction (solid magenta line). The arrow and gray shaded area indicate where excess dye delays the onset of turnover measurement, leading to an overestimation error. **b**, Simulation with different dye-protein ratios (x-axis) and true lifetimes (y-axis). The estimated lifetime is colored. Undersaturation (left side <1 dye/protein ratio) causes worse errors than dye excess (right side >1 dye/protein ratio) and longer-lived proteins (>10 h) are better estimated than short-lived ones. **c,** Schematic of the procedure for measuring the turnover of nuclear MeCP2-HT protein in a knock-in mouse model. Three dyes were used to measure multiple protein-turnover intervals. After perfusion and dissection, coronal sections were stained with IF to identify different cell types, while DAPI was used as a nuclear marker. **d,** Example field of view showing all JF dyes (left 3 panels) imaged with an example NeuN stained coronal section (4th panel) to identify neurons alongside all nuclei (DAPI; 5th panel). After segmentation of NeuN positive nuclei (6th panel), segmented nuclei were colored by lifetime using the sum of the two *in vivo* injections as the pulse (JF_{669}+JF_{552} / JF_{669}+JF_{552}+JF_{608}). **e,** Example coronal sections from 2 animals showing the consistency of the lifetime estimate for the same AP section (compare left and middle panel) and differences across brain regions, most notably the longer lifetime in the cerebellum (compare middle and right panels). **f,** lifetime means and bootstrap confidence intervals for CCF aligned brain regions of MeCP2.

Figure 2 – PSD95 turnover depends on experience

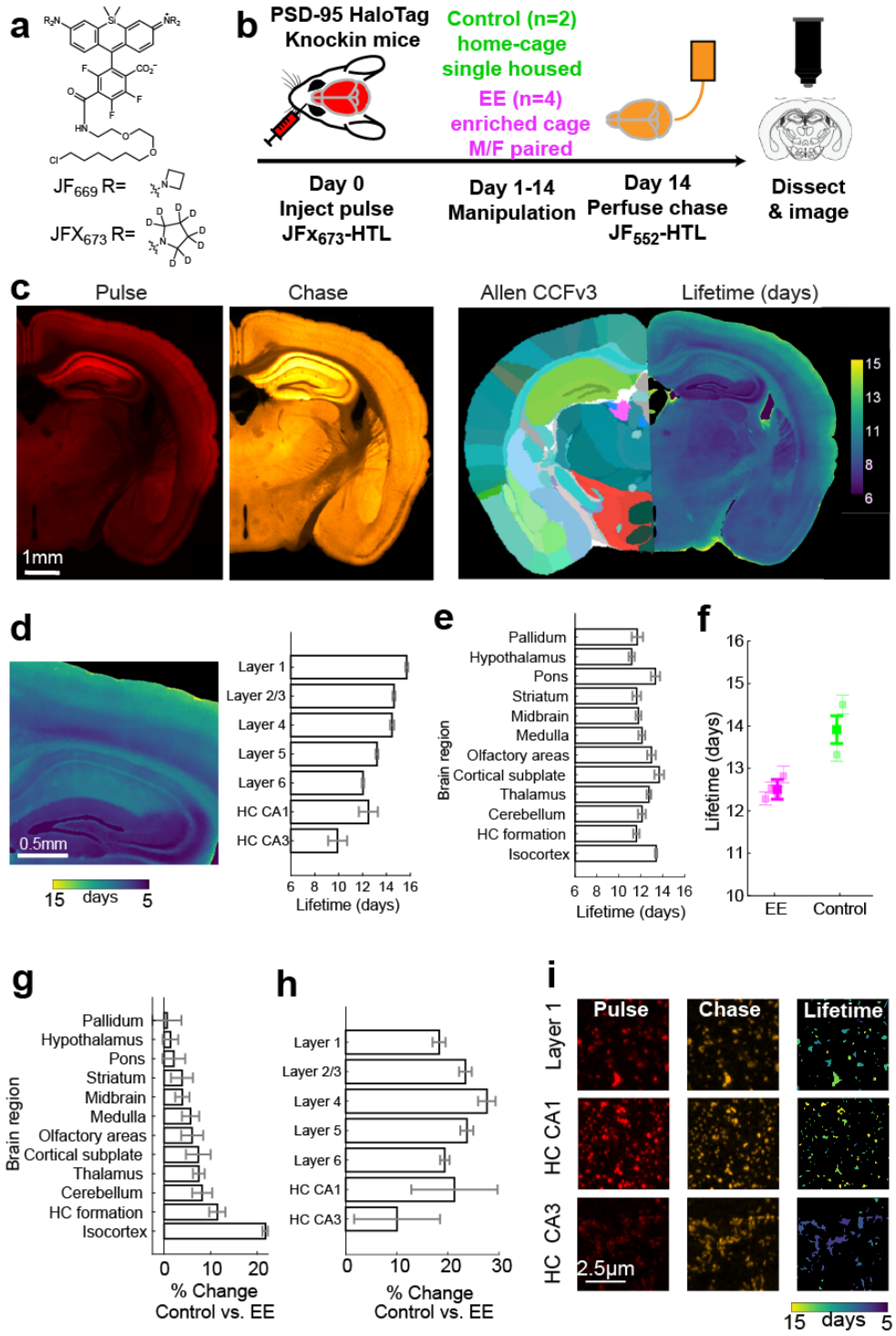

a, Structure of JF_{669}-HTL and the new JFX_{673}-HTL. Note the replacement of deuterium and extra carbon in the R position. **b,** Schematic of the procedure for measuring the turnover of synaptic

PSD95-HT protein in a knock-in mouse. After initial injection of the new JFX_{673} animals were separated to be single housed (n=2) or male/female paired in an enriched environment (EE, n=4) for 14 days. At the end of 2 weeks the animals were perfused with JF_{552}, sectioned, imaged, and aligned to the Allen Institute CCFv3. **c,** Example coronal section showing the pulse (left panel), chase (middle panel), and calculated lifetime aligned to the Allen CCFv3 (right panel). **d,** Left: zoom in of the image from panel c. Note the gradient in lifetime separating the CA1 *stratum radiatum* (long lifetime) and CA1 *stratum lacunosum moleculare*, dentate gyrus *stratum moleculare* and hilus (all short lifetime). Right: Average lifetime of different cortical layers and subfields of the hippocampus (HC). **e**, Average lifetime for 12 large brain regions. **f,** Average lifetime of the 4 animals in EE (magenta) and control conditions (green). EE increased protein turnover and shortened the average lifetime of PSD95. Individual animals in lighter colors. **g,** Percent change in control vs. EE animal across cortical layers. **h,** same as **g** for 12 different brain regions. **i,** Example images using Airyscan imaging of ExM tissue (max projection of 5 z planes 0.3 um apart) from layer 1 (top row), HC CA1 subfield (middle row) and basal dendrites of CA3 (bottom row) showing both pulse (left columns), chase (middle columns) and lifetime (left columns).